How do tradeoffs in satellite spatial and temporal resolution impact snow water equivalent reconstruction?

Edward H. Bair[1], Jeff Dozier[2], Karl Rittger[3], Timbo Stillinger[1], William Kleiber[4], and Robert E. Davis[5]

[1]Earth Research Institute, University of California, Santa Barbara, CA USA 93106
[2]Bren School of Environmental Science and Management, University of California, Santa Barbara, CA USA 93106
[3]Institute of Arctic and Alpine Research, University of Colorado, Boulder, CO 80309
[4]Department of Applied Mathematics, University of Colorado, Boulder, CO 80309
[5]Cold Regions Research and Engineering Laboratory, Hanover, NH USA 03755

Correspondence to: Edward H. Bair (nbair@eri.ucsb.edu)

Abstract

Given the tradeoffs between spatial and temporal resolution, questions about resolution optimality are fundamental to the study of global snow. Answers to these questions will inform future scientific priorities and mission specifications. Heterogeneity of mountain snowpacks drives a need for daily snow cover mapping at the slope scale (≤ 30 m) that is unmet for a variety of scientific users, ranging from hydrologists to the military to wildlife biologists. But finer spatial resolution usually requires coarser temporal or spectral resolution. Thus, no single sensor can meet all these needs. Recently, constellations of satellites and fusion techniques have made noteworthy progress. The efficacy of two such recent advances is examined: 1) a fused MODIS - Landsat product with daily 30 m spatial resolution; and 2) a harmonized Landsat 8 - Sentinel 2A/B (HLS) product with 3-4 day temporal and 30 m spatial resolution. State-of-art spectral unmixing techniques are applied to surface reflectance products from 1 & 2 to create snow cover and albedo maps. Then an energy balance model was run to reconstruct snow water equivalent (SWE). For validation, lidar-based Airborne Snow Observatory SWE estimates were used. Results show that reconstructed SWE forced with 30 m resolution snow cover has lower bias, a measure of basin-wide accuracy, than the baseline case using MODIS (463 m cell size), but greater mean absolute error, a measure of per-pixel accuracy. However, the differences in errors may be within uncertainties from scaling artifacts e.g., basin boundary delineation. Other explanations are 1) the importance of daily acquisitions and 2) the limitations of downscaled forcings for reconstruction. Conclusions are: 1) spectrally unmixed snow cover and snow albedo from MODIS continue to provide accurate forcings for snow models; and 2) finer spatial and temporal resolution through sensor design, fusion techniques, and satellite constellations are the future for Earth observations, but existing moderate resolution sensors still offer value.

1. Introduction

Mountain snowpacks are challenging for remote sensing because they change rapidly. Moderate resolution sensors such as MODIS and VIIRS image Earth daily, but at resolutions (463 m - 750 m) that cannot resolve slope scale features of interest to a variety of scientific users ranging from hydrologists (Blöschl, 1999), to the military (Vuyovich et al., 2018), to wildlife biologists (Conner et al., 2018). Finer resolution multispectral sensors such as Landsat 8/9 provide spatial resolutions of 30 m, but at 16-day revisits, during which time the snow cover can change considerably. Because of cloud cover, useable optical imagery with such infrequent revisits can be months apart. Recognizing that no single satellite/instrument can provide fine spatial and temporal resolution, constellations of satellites with coordinated overpass times have emerged. Two examples are the Sentinel 2 A/B and Landsat 8/9 pairs. For optical bands, the Sentinels image Earth every 5 days at 20 m, and Landsats 8/9 image Earth every 8 days at 30 m. The Harmonized Landsat 8/9 Sentinel 2 (HLS) product (Claverie et al., 2018) improves the average revisit time to 3-4 days at 30 m spatial resolution.

Effects of snow cover estimates at finer resolution have been examined in a few studies, showing a wide range of improvements in errors. In comparing snow cover depletion curves from Landsat MSS (80 m pixels; 16-day repeat) and AVHRR imagery (1100 m pixels; daily repeat), Baumgartner et al. (1987) found that AVHRR tended to overestimate snow cover where it was patchier (lower elevations) and underestimate snow cover where it was more widespread (higher elevations), relative to MSS. They concluded that AVHRR imagery could be used to fill in temporal gaps in depletion curves generated from Landsat MSS. Luce et al. (1998) compared a spatially explicit SWE model at 30 m with single and two point models for a small basin in Idaho. The 30 m model showed significantly lower errors than the single and two point models. Cline et al. (1998) examined the effect of upscaling the spatial resolution of a DEM and snow cover in an energy balance SWE model at a range of resolutions: 30, 90, 250 and 500 m. Positive biases in the coarser resolution estimates arising solely from basin delineation artifacts were reported, thus the authors advise using vector basin outlines (as was done in Section 2.5). When these artifacts were corrected, the SWE volumes at 90 m were overestimates while those at coarser resolutions were underestimates. Blöschl (1999) examined scaling issues in snow hydrology and shows that pixel sizes of a few m are needed to accurately capture basin-scale SWE. Turpin et al. (2000) examined snow cover maps derived from AVHRR and Landsat TM (30 m resolution; 16-day repeat) and report discrepancies, also finding that AVHRR failed to resolve patchy snow compared to TM. Durand et al. (2008) were the first to create a fused MODIS and Landsat product. For the coarse resolution product they used binary snow cover from MODIS (Hall et al., 2002). For the fine resolution product they used Landsat 7 ETM+ surface reflectance in a spectral unmixing algorithm (Painter et al., 2003). The authors then used a linear program, constrained to match the ETM+ fractional snow-covered area (fsca) imagery while also matching the daily changes in fsca observed by MODIS. Applying their linear program to the upper Rio Grande, the authors found differences in fsca between the ETM+ fsca, the MODIS fsca, and the fused product. When run through a snow reconstruction model, these differences equated to a 51% reduction in mean absolute error (MAE) and a 49% reduction in bias for SWE using the fused snow cover versus the ETM+ snow cover. Using the same reconstruction model, Molotch and Margulis (2008) report a 23% MAE in SWE

2

using ETM+ snow cover, versus a 50% MAE in SWE using MODIS snow cover, and 89% MAE using AVHRR snow cover. Rittger et al. (2013) examined spectrally unmixed snow cover from ETM+ (similar to the approach in Painter et al., 2009) and several approaches for mapping snow cover from MODIS, including spectral mixture analysis (Painter et al., 2009). They found that ETM+ mapped consistently more patchy snow cover than the MODIS approaches, suggesting fewer false negatives and thus a greater recall statistic. Winstral et al. (2014) examined scale in a snow energy balance model at a range of spatial resolutions and find that 100 m spatial resolution is needed to accurately simulate snow melt. Contrary to Cline et al. (1998), Schlögl et al. (2016) report that SWE increases with DEM resolution in two alpine basins. Similarly, Baba et al. (2019) used an energy balance model with a DEM at 8-1000 m and report good agreement with fine resolution snow cover maps up to 250 m, but a loss in agreement at coarser resolution, likely due to excessive smoothing of topographic effects. Rittger et al. (2021) used a random forest to fuse spectrally unmixed snow cover from MODIS with Landsat 5 and 7 ETM+. The authors' comparisons show sharper snowlines (transition from no snow to fully snow covered) in the Landsat and fused imagery compared to MODIS, again indicating that Landsat may have greater recall than MODIS in this difficult to validate region. Bouamri et al. (2021) examined differences between snowmelt models with and without solar radiation represented in the Atlas Mountains of Morocco. Although the models with solar radiation better simulated the snowcover used for validation, aggregating the simulated snow cover from 100 to 500 m suppressed those improvements. In summary, many studies have compared coarse and fine resolution snow cover, but only three studies to our knowledge (Cline et al., 1998; Durand et al., 2008; Molotch and Margulis, 2008) have examined the impact of resolution on SWE reconstruction, all finding significant improvements from finer spatial resolution. Since those studies, considerable advances have been made in SWE reconstruction techniques (Bair et al., 2016; Rittger et al., 2016) as well as snow cover (Stillinger et al., 2023) and albedo mapping (Bair et al., 2019), hence the justification for revisiting the effects of spatial and temporal resolution.

2. Approach

Three daily snow cover estimates were used to force a SWE reconstruction model at two spatial resolutions: a baseline at 463 m using MODIS with the Snow Property Inversion from Remote Sensing (SPIReS, Section 2.1, Bair et al., 2021), and two 30 m estimates, one from the Harmonized Landsat-Sentinel (HLS) surface reflectance product (also using SPIReS, Section 2.2), the other from Snow Covered Area and Grain Size (SCAG)-Fusion (Section 2.3). The period covered is 1 Jan 2018 to 31 Dec 2020, limited by the intersection of the availability of the SCAG-Fusion and the HLS. The domain is the Tuolumne River Basin above the Hetch Hetchy Reservoir in the Sierra Nevada USA because of the availability of Airborne Snow Observatory (Painter et al., 2016) estimates of SWE for validation. This approach rests on the hypothesis that 1) fsca and 2) snow albedo are the two most important variables in SWE reconstruction (see Section 2.4). The importance of fsca in SWE reconstructions can be traced to several studies (e.g., Durand et al., 2008; Molotch and Margulis, 2008). The importance of snow albedo in SWE reconstructions is shown in Bair et al. (2019).

2.1. SPIReS-MODIS

The baseline case uses SPIReS to map snow cover from MODIS at 463 m daily resolution, although the effective pixel size can be up to 5× as large for off nadir acquisitions (Wolfe et al., 1998; Dozier et al., 2008). The MOD09GA daily surface reflectances (Vermote et al., 2015) are unmixed into fsca and properties used to model albedo (grain size and dust concentration). These estimates are then run through a series of filters including persistence filters for clouds and time-based smoothing/interpolation.

2.2. SPIReS-HLS

One daily 30 m snow cover product used also comes from the SPIReS approach applied to the HLS. As the first snow mapping application, to our knowledge, of HLS data. Thus, we describe the workflow in more detail than SPIReS-MODIS. The Tuolumne River Basin above Hetch Hetchy Reservoir straddles two Sentinel tiles, so HLS version 1.4 multi-band HDF files from both tiles were downloaded (https://hls.gsfc.nasa.gov/). For calendar years 2018-2020, four combinations of products were downloaded: two tiles (11SKB,11SKC); and two products – S30 (Harmonized Sentinel-2 MSI) and L30 (Harmonized Landsat-8 OLI). We attempted to download the newer HLS version 2.0 from NASA Earthdata Search, but as of this writing, the S30 product for those tiles only extends back to 2020 Sep 23 because of daily limits on the number of Sentinel-2A/B scenes that can be downloaded by NASA from ESA for reprocessing. Seven bands covering visible through shortwave-infrared wavelengths were used from each sensor: 1-4, 8A, and 11-12 for S30; 1-7 for L30. Mean local solar geometry was obtained from the accompanying header files. The multi-band images were stacked, mosaiced, and cropped to the basin to form a $1119 \times 1297 \times 7 \times 311$ 4D data structure, with dimensions of rows, columns, bands, and time. Each Landsat has a 16-day revisit, thereby providing imagery at 8-day intervals for each tile, and each Sentinel has a 10-day revisit, providing imagery at 5-day intervals. Thus, combined revisits ranged from around 1 day to 10 days with a mean of 3.5 days (Figure 1). Theoretical revisit times estimated before Landsat 9 was launched (Li and Roy, 2017) for a three-satellite constellation at this basin's latitude shows a mean of 3.8 days, with a minimum of less than one day and a maximum of 7.0 days. There are only 4 revisit times greater than 7 days shown in Figure 1; all other observations lie within the theoretical revisit times.
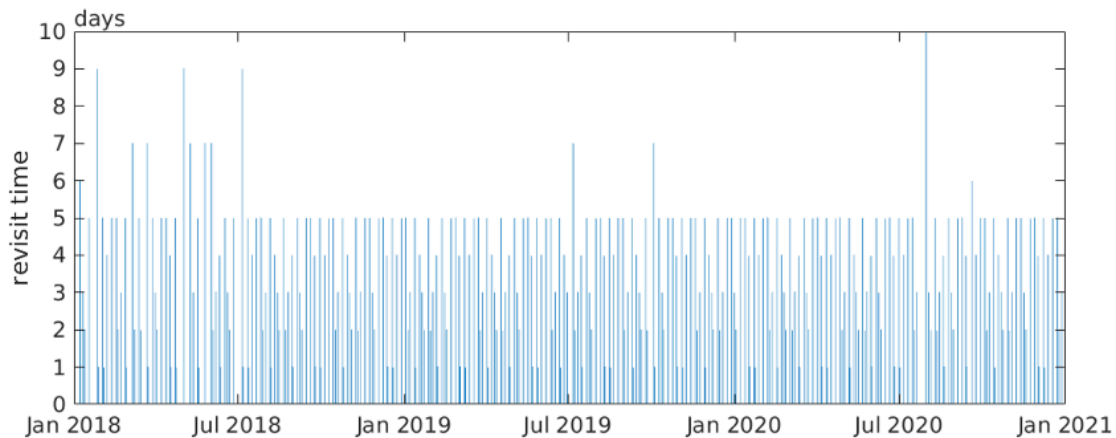
4

Figure 1:

Revisit times covering the Tuolumne River Basin above Hetch Hetchy Reservoir for the HLS S30 and L30 combined.

120   Red/green/blue band imagery for each day was examined visually. Days with clouds or incomplete spatial coverage over the watershed (many images have large areas with no data) were discarded. After filtering, 156 or about half of the days were kept. The minimum, median, and maximum time spacings between acquisitions after filtering were 1, 5, and 40 days. The SPIReS spectral unmixing approach was then applied to these filtered surface reflectances as described for Landsat 8 OLI in Bair et al. (2021), yielding the variables fsca, snow grain size, and dust concentration. A per-pixel spline interpolation was
125   applied to each of the variables in the time dimension to make them continuous, covering all days from 2018-2020.

2.3. SCAG-Fusion

A second daily 30 m snow cover product used was a MODIS-Landsat fusion, created using two random forests for classification and regression based on previous work (Rittger et al., 2021) but retrained using Landsat 8 OLI data. Standard cloud masks (Foga et al., 2017) were used to select the 100 most cloud free Level 2 surface reflectance images (USGS, 2021)
130   for dates spanning Mar 2013 to Mar 2021 (Figure 2). Winter months had fewer training data than summer months. Six scenes were manually removed after visual inspection of red/green/blue imagery. Because the initial filtering did not remove all clouds, a second cloud filtering step with Superpixels and Gabor filtering was used (Stillinger, 2019). This second step removed all the clouds, but removed some snow cover as well. These filtered Landsat 8 surface reflectances along with MODIS MOD09GA surface reflectances were unmixed into fsca and snow surface properties that affect albedo (Painter et al., 2009;
135   Painter et al., 2012). This SCAG spectral unmixing differs from the SPIReS approach; it finds the best fit from an endmember library for the snow-free parts of the pixel, whereas SPIReS uses an empirical snow-free endmember. There are other differences in the treatment of light absorbing impurities, filtering, and time-space smoothing (Rittger et al., 2020). For more details and a recent comparison between SPIReS, SCAG, and all other accessible snow mapping algorithms see Stillinger et al. (2022). Estimates of fsca and snow surface properties that affect albedo i.e., grain size and visible albedo degradation were

5

140   used as training data. Physiographic variables, including solar illumination and land classification were used as predictors. The two-step approach consists of an initial model that classifies pixels into 3 cases: (1) 0%, (2) 100%, or (3) 1-99% fsca. For case (3), a second regression random forest was used to estimate fsca on the 1-99% interval. This two-step classification-regression approach was found to be less biased at predicting 100% snow covered pixels than using a single-step random forest predicting 0-100% fsca.
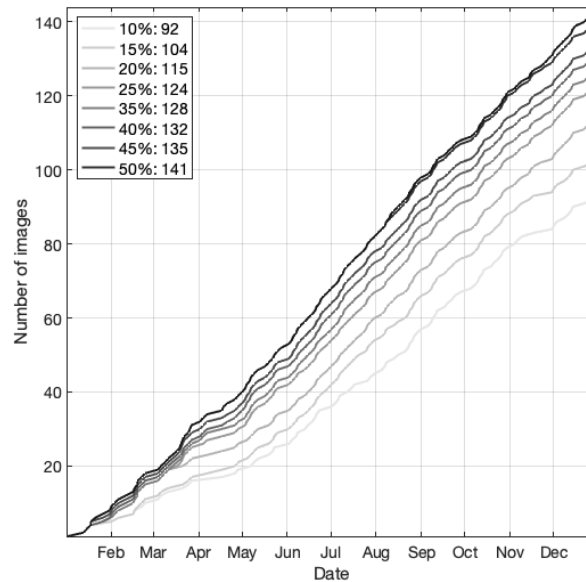
145

Figure 2:

Cumulative number of images over 8 years acquired from Landsat 8. Lighter to darker lines indicate increasing cloud coverage from 10-50%. Numbers after the cloud cover percentage in the legend correspond to the total number of images. Images with 12% or less cloud cover were selected.

150   **2.4. Parallel energy balance**

At an hourly timestep, the Parallel Energy Balance model ParBal (Bair et al., 2016; Rittger et al., 2016; Bair et al., 2018) downscales state and flux variables solving for the surface snow energy balance. The computed melt is multiplied by the fsca and summed backward from end-of-melt to peak SWE for each pixel to estimate SWE on the ground throughout the melt season. Evaluations of ParBal (Bair et al., 2016; Bair et al., 2018) forced with snow cover from the MODSCAG approach
155   (Painter et al., 2009; Rittger et al., 2020) show a mean absolute error (MAE) of 22-26% using SWE from ASO for validation. There are two significant changes to ParBal here. 1) U and V wind component forcings use the hourly MERRA-2 (Global Modeling and Assimilation Office (GMAO), 2015) data instead of N/GLDAS-2 (Rodell et al., 2004; Xia et al., 2012). Using U & V components with global forcings allows for terrain-based wind downscaling using curvature and slope (Liston et al., 2007), whereas GLDAS only provides wind speed. 2) A new estimate of SWE on the ground, called hybrid SWE, leverages
160   GLDAS SWE (the GLDAS NOAH 3-hour 0.25º v2.1 model was used) and captures the accumulation phase. Previously,

ParBal estimates were limited to the ablation phase only. The concept is to identify GLDAS pixels with similar snow cover duration as the fine-scale fsca pixels, find the peak SWE day from those GLDAS pixels, then scale the GLDAS estimates by the ParBal SWE estimate on that peak day. This process is repeated for every fine-scale pixel. The GLDAS SWE, SWE_{GLDAS}, is extracted for the domain, in this case a bounding box covering the Tuolumne River Basin above Hetch Hetchy Reservoir.

165 Pixels with the same snow cover duration are identified as

$$SWE^{*}_{GLDAS} = \left(SWE_{GLDAS,\Delta t_1} > 0, fsca_{\Delta t_1} > 0\right) \& \left(SWE_{GLDAS,\Delta t_2} = 0, fsca_{\Delta t_2} = 0\right) \tag{1}$$

where the asterisk denotes the selected pixels and fsca is from the fine-scaled product i.e., Section 2.1 - 2.2. The Δt_1 and Δt_2 indicate different time periods. Because there can be multiple pixels with matching snow cover duration, the daily mean of SWE^{*}_{GLDAS} is taken. The maximum value of that daily mean and its index $imax$ are computed. A scaling coefficient c is calculated as

$$c = SWE_{ParBal,imax}/max(\overline{SWE^{*}_{GLDAS}}) \tag{2}$$

170 where $SWE_{ParBal,imax}$ is the value of the reconstructed SWE from ParBal (Eq. 2 in Bair et al., 2016) at the time $imax$ and the overbar denotes an average. The following case can arise

$$c = 0, SWE_{ParBal,imax} = 0, (SWE_{GLDAS} > 0) \wedge (fsca > 0). \tag{3}$$

For example, this case can occur when ParBal models all the mass loss via sublimation. For this case, SWE_{GLDAS} is used when fsca > 0. Otherwise, the hybrid SWE prior to the peak is set at day i as

$$SWE_{hybrid,i} = c \times SWE_{GLDAS,i}, i \leq imax. \tag{4}$$

This scaling can cause unrealistic daily increases and decreases in SWE; thus a smoothing spline is applied. This hybrid

175 SWE has yet to be evaluated throughout the accumulation season, but comparison with the reconstructed SWE during the ASO acquisitions show negligible differences, indicating at least the $imax$ estimate is occurring roughly at the right time of year since the all of the ASO flights examined here took place during the ablation season (with the exception of 13 Apr 2020, Section 3). Figure 3 shows this hybrid GLDAS and reconstructed SWE for an example pixel in WY 2019. ParBal was run with each of the snow cover forcings, holding all other inputs constant.
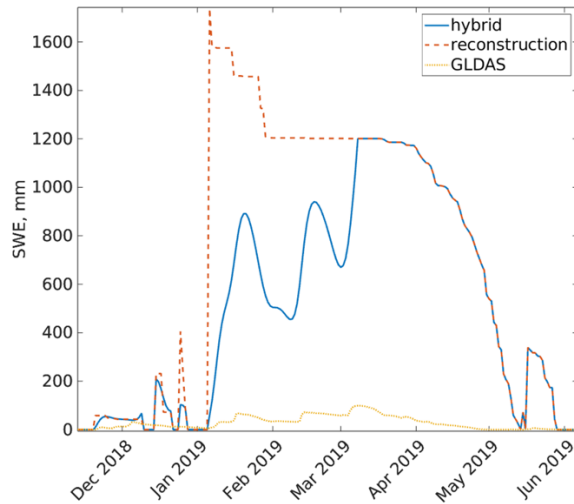
180

Figure 3:

Hybrid SWE estimates for the accumulation season combining reconstruction and GLDAS for an example pixel using the SPIReS-HLS snow cover.

2.5. Airborne Snow Observatory

185   ASO 50 m SWE estimates for the Tuolumne River Basin above the Hetch Hetchy Reservoir, which is the most sampled

basin by ASO, were downloaded from the National Snow and Ice Data Center for 2018 and 2019 and from ASO Inc. for

2020 (Table 1). The number of acquisitions per year ranged from two (2018) to four (2019) with a total of nine. Accuracy of

ASO measurements at the basin scale cannot be estimated directly from data, since there is no better method for validation,

but since 2021, ASO has provided basin-wide uncertainty estimates on their reports available on their website

190   (https://www.airbornesnowobservatories.com), mostly based on uncertainty in modeled density, with a small uncertainty in

depth. The reported mean basin-wide uncertainty in SWE for ASO flights the entire Tuolumne River Basin for 2021 and

2022 is $\pm 4\%$, so we assume similar errors in 2018-2020 and use that uncertainty estimate.

Year	Name	Mean SWE, mm
2018	23 Apr	418
	28 May	127
2019	17 Apr	1095
	3 May	840
	13 Jun	441
	5 Jul	111
2020	13 Apr	293
	7 May	191

8

	21 May	128

Table 1:

Tuolumne River Basin above Hetch Hetchy Reservoir SWE estimates for 2018-2020 for the Airborne Snow Observatory.

2.6. Analysis

The ASO images were resampled from a cell size of 50 m to 2000 m (4× the MODIS resolution) and 120 m (4× the Landsat resolution), using a mean-preserving technique with a weighted resampling covering the image (mapresize, MathWorks, 2022). The ASO images were kept in their native UTM 11N projection. The upscaled cell sizes account for geolocational and sensor-to-sensor uncertainty of 1-2 pixels for MODIS and Landsat/Sentinel-2 (Tan et al., 2006; Storey et al., 2016). The ASO dates in Table 1 were extracted for each of the three SWE reconstructions. Then, the matched baseline SPIReS-MODIS images were upscaled from 463 m to 2000 m and reprojected from a sinusoidal projection to UTM 11N. The matched MODIS-Landsat fusion and SPIReS-HLS images were upscaled from 30 m to 120 m but kept in their native UTM 11N projection. Vectors of the Tuolumne River Basin above Hetch Hetchy Reservoir were obtained from ASO Inc. These vectors were then converted into coarse resolution masks of the basin. Water bodies and other areas with no data in either the ASO images or in the SWE reconstructions were removed from the masks. Areas outside of the masks were then set to null values. These common masks were applied to the upscaled SWE reconstruction and ASO images such that areas outside the masks were set to null values. The upscaled ASO images were compared with the upscaled SWE reconstruction images. The following error statistics were computed for a given date: bias as a measure of basin-wide error, relative bias normalized by ASO mean SWE, mean absolute error (MAE) as an unweighted measure of per-pixel error, and relative MAE normalized by ASO mean SWE:

$$\text{bias} = \frac{1}{N} \sum_{j=1}^{N} \text{SWE}_{ParBal,j} - \text{SWE}_{ASO,j} \tag{5}$$

$$\text{relative bias} = \frac{\frac{1}{N} \sum_{j=1}^{N} \text{SWE}_{ParBal,j} - \text{SWE}_{ASO,j}}{\frac{1}{N} \sum_{j=1}^{N} \text{SWE}_{ASO,j}} \tag{6}$$

$$\text{mean absolute error} = \frac{1}{N} \sum_{j=1}^{N} \left| \text{SWE}_{ParBal,j} - \text{SWE}_{ASO,j} \right| \tag{7}$$

$$\text{relative mean absolute error} = \frac{\frac{1}{N} \sum_{j=1}^{N} \left| \text{SWE}_{ParBal,j} - \text{SWE}_{ASO,j} \right|}{\frac{1}{N} \sum_{j=1}^{N} \text{SWE}_{ASO,j}} \tag{8}$$

where N the total number of pixels and j is an individual pixel. Mean values of the four error statistics were also averaged by year. MAE is used instead of Root Mean Squared Error because it evenly weights errors which is preferred when comparing modeled values (Cort and Kenji, 2005) i.e., ParBal to ASO, neither of which directly measure SWE.

2.7. Snow albedo errors

Errors in snow albedo directly impact the accuracy of reconstructed SWE (Bair et al., 2019). However, for the spectral unmixing approaches used here, the albedo errors are low, evaluated using terrain-corrected measurements from Mammoth Mountain (e.g., Bair et al., 2022), only 23 km from Mount Lyell, the highest point in the Tuolumne River Basin. For example, from water years 2017-2019, the Root Mean Squared Error (RMSE) for MODIS-SPIReS, calculated using the best value for a 3×3 neighborhood around the validation site, is 2.3% with no bias (Table 2). These albedo errors are similar to the accuracy of the HDRF surface reflectance products, evaluated over dark targets (Vermote et al., 2016; Bair et al., 2022). These improvements in remotely sensed snow albedo over previous assessments, showing RMSE values of 4.6 to 4.8% with 0.7-1.3% bias for MODIS (Bair et al., 2019; Bair et al., 2021), come from improved cloud snow discrimination filters and adjustments to thresholds such as the minimum grain size for dirty snow (Section III-J of Bair et al., 2021).

Water year	Bias, %	RMSE, %
2017	-0.8	2.2
2018	-0.3	2.4
2019	1.0	2.4
mean	**0.0**	**2.3**

Table 2:

Snow albedo from SPIReS-MODIS validated with terrain-corrected snow albedo from the CUES site on Mammoth Mountain (Bair et al., 2015) taken using an adjustable arm to keep the radiometers 1 m above the snow surface (Bair et al., 2022). A best of 3×3 pixel neighborhood was used to account for geolocational uncertainty.

230   We are not dismissing errors in albedo, as these remotely-sensed snow albedo errors can lead to 5-11 % MAE for reconstructed SWE (Bair et al., 2019), but without independent measurements of spatially distributed albedo, we lack validation data for further error evaluation.

3.   Results and discussion

Basin-wide mean SWE errors are shown in Figure 5a-c and in Table 3. The lower mean MAE, by 10-14% (bold in Table
235   3) from SPIReS-MODIS is perhaps the most intriguing result, contradicting the result of previous studies (Section 1) which find that finer spatial resolution estimates of snow cover reduce SWE errors. The reduction of 4-5% relative bias from the two 30 m snow cover forcings compared to MODIS agrees with the previous findings, although the magnitudes of the reductions are smaller than in previous studies (e.g., Durand et al., 2008). To test if the lower MAE from MODIS are resolution artifacts, the SPIReS-HLS and SCAG-Fusion products were also upscaled to 2000 m cell sizes instead of 120 m. For mean values over
240   all water years for these upscaled comparisons (Table A1), SPIReS-MODIS still had the lowest relative MAE, but the SCAG-Fusion relative bias dropped to 3% while the SPIReS-HLS relative bias increased to 9%, equal to SPIReS-MODIS. These results suggest that the evaluations are sensitive to the upscaled pixel size, meaning that the differences in errors across the three SWE reconstructions may be within uncertainty bounds introduced by upscaling artifacts such as basin delineation. For example, in the UTM 11N projection, the shapefile obtained from ASO Inc. for the Tuolumne River Basin above Hetch Hetchy
245   Reservoir has an area of 1175 km^2; a raster of the basin at 120 m has an area of 1153 km^2 (-1.8%) while a raster at 2000 m has an area of 1132 km^2 (-3.6%). Even when using vector basin outlines, as suggested by Cline et al. (1998), these artifacts are inherent in the discretization of geospatial data and cannot be eliminated.

Another explanation for the poorer MAE performance from SPIReS-MODIS is that some spatial variation in topography is lost with the coarser resolution. To test this hypothesis, a semi-variogram of the terrain slope is examined, as in Baba et al.
250   (2019). The semi-variogram shows a flattening around 500 m, indicating that variation in topography, which can manifest in topographically driven variables such as direct solar illumination, is poorly captured at MODIS and coarser spatial scales. This semi-variogram analysis confirms the above hypothesis. Further, downscaling coarse scale reanalysis products (Winstral et al., 2014) e.g., the downwelling radiation from Clouds and Earth's Radiant Energy System (Rutan et al., 2015) at 1º spatial

resolution, has inherent limitations, often due to clouds (Lapo et al., 2017). Important to note is that ParBal does not use

255 precipitation as a forcing and thus does not suffer from well-known biases and downscaling issues (Raleigh et al., 2015; Pflug et al., 2021).
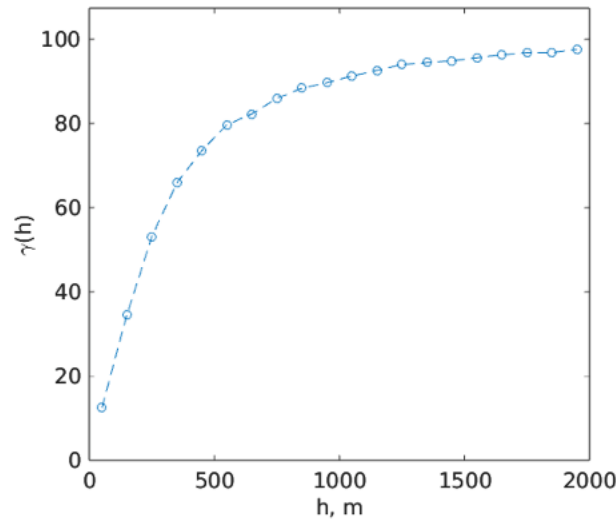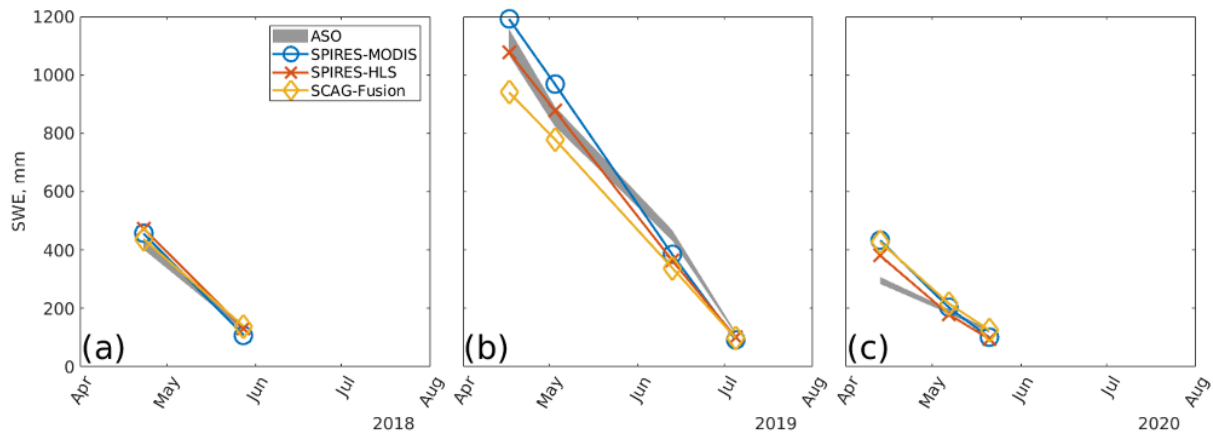

Figure 4:

Semi-variance of terrain slope of the Tuolumne River Basin above Hetch Hetchy. The slope of the semivariance (not the terrain
260 *slope itself) shows a flattening around 500 m, or about the MODIS pixel size.*

Alternatively, the lower MAE may indicate the importance of daily imaging from MODIS compared to the HLS snow cover, which had median gap of 5 days between revisits after filtering for clouds. In contrast, the SCAG-Fusion used daily MODIS snow cover in the prediction and training steps indicating it suffers from errors not related to revisit time.


265 Figure 5:

Basin-side SWE values by date for the three SWE reconstructions (a-c) compared to Airborne Snow Observatory estimates.
Assumed uncertainty in the ASO measurements is ±4% (Section 2.5) and is shaded in gray.

12

Name	Year	Bias, mm	Relative Bias, %	MAE, mm	Relative MAE, %
SPIReS-MODIS	2018	9	3	87	32
	2019	26	4	168	26
	2020	43	21	95	47
	mean	**26**	**9**	**117**	**35**
SPIReS-HLS	2018	27	10	135	49
	2019	-24	-4	201	32
	2020	12	6	111	54
	mean	**5**	**4**	**149**	**45**
SCAG-Fusion	2018	13	5	122	44
	2019	-89	-14	264	42
	2020	50	24	123	60
	mean	**-9**	**5**	**170**	**49**

Table 3:

*Error statistics by year for the three SWE reconstructions. Mean values for all years are shown in **bold**. More detailed errors by date are given in the Appendix.*

An example of the SWE modeled by ASO on 4 May 2019 and the three reconstructions is shown in Figure 6. The spatial distribution of the SWE from ASO matches well with all the reconstructions. Differences between the reconstructions can be seen around Mount Lyell, at the southernmost part of the basin. The ASO SWE shows high variability here, ranging from a few hundred mm of SWE to over 2000 mm, while the reconstructions model consistently higher amounts of SWE. The overestimates here are likely related to false-positive classifications for snow. Especially late in the summer, when melt rates are high, these false-positives can lead to substantial overestimates of SWE during reconstruction (Slater et al., 2013). A close examination of the mostly snow-free areas in gray shows that only the SPIReS-HLS reconstructions replicate the small patches of thin snow in this area, likely because the SPIReS-HLS snow cover was not smoothed to the same degree as the SPIReS-MODIS or SCAG-Fusion, which both use heavy smoothing to reduce noise and smearing from MODIS.
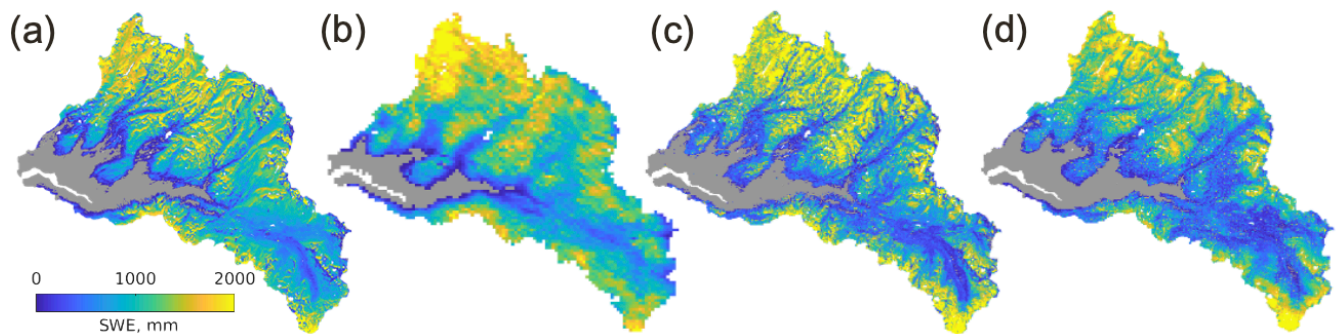
Figure 6:

SWE in the Tuolumne River Basin above Hetch Hetchy Reservoir for 4 May 2019 modeled by the Airborne Snow Observatory (a) along with reconstructions from SPIReS-MODIS (b), SPIReS-HLS (c), and SCAG-Fusion (d).

Errors are further examined by date (Figure 7 and Table A2). Except for 13 Apr 2020, the bias across all the products is
285 between -20 and 20% (Figure 7a). Figure 8 shows a snow pillow (weighing gauge, California Department of Water Resources station code DAN, elevation 2987 m) and that the ASO flight on 13 Apr 2020 is the only flight in this study that occurred prior to peak SWE. Overestimates of SWE prior to its peak are a limitation of SWE reconstruction. The hybrid SWE method (Section 2.4) extends SWE estimates throughout the year, but the high biases found on this date are not surprising, because snow melt occurred prior to the flight and snow accumulation occurred after the flight. Note the missing data on DAN after 3 May 2018
290 in Figure 8, but the CUES snow pillow, which is nearby and at a similar elevation (2940 m), shows clear ablation during May 2018.

Examination of the per-pixel MAE (Figure 7b) shows that the SPIReS-HLS product has the most consistent values, with the two approaches that used MODIS data (SPIReS-MODIS and SCAG-Fusion), showing more variability, perhaps again due to the smoothing needed for the relatively noisy MODIS data or the fact that SCAG-Fusion was trained using more data outside
295 the test period (March 2013 to December 2017 and January 2021 to March 2022) than within it (January 2018 to January 2021).
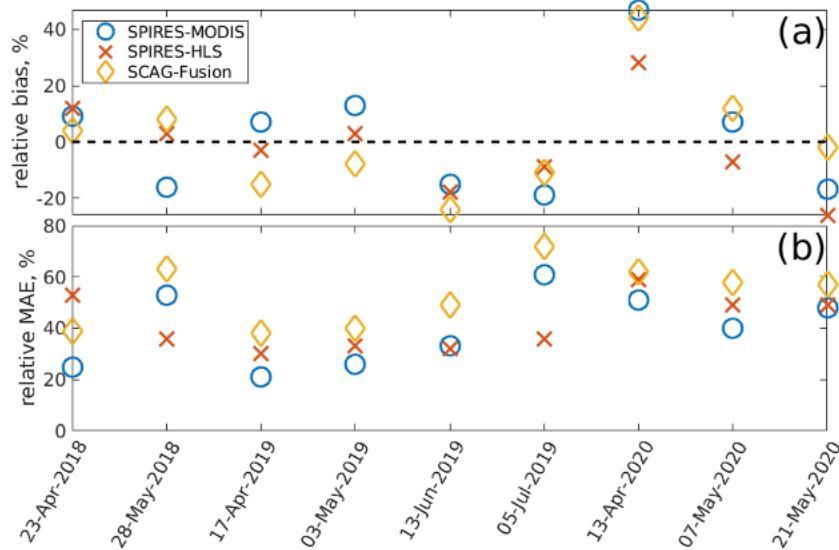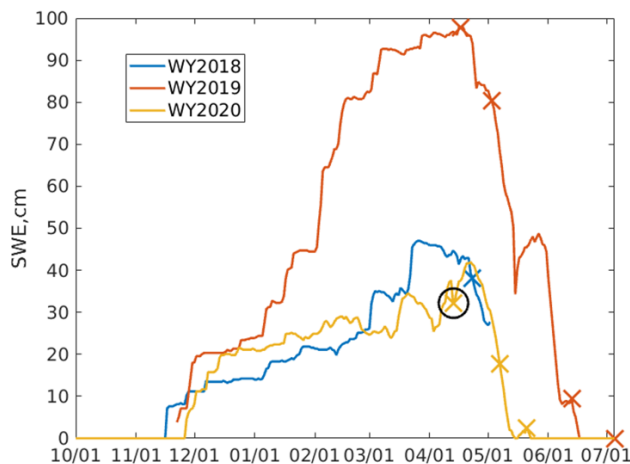

Figure 7:
SWE errors by date for the three SWE reconstructions. The relative bias is shown in (a), the relative MAE in (b).

14

300

Figure 8:

Snow pillow DAN in the Tuolumne River Basin showing daily SWE. The X markers show the dates of ASO flights. Circled is the 13 Apr 2020 ASO flight, which is the only flight that occurred prior to peak SWE. The pillow was not reporting from 3 May 2018 to 21 Nov 2018, but a nearby snow pillow shows consistent ablation in May 2018.

305   Stillinger et al. (2022) show that errors in snow cover mapping depend on canopy cover, having to do with how much areal snow is viewable at the pixel scale by a sensor, which affects the accuracy of the SWE reconstructions (Bair et al., 2016). Thus, we examine errors in the SWE reconstructions, binned by canopy cover fraction, for each snow cover forcing. The bin centered at 5% (range: 0 to 9.9%) canopy cover (containing 46-60% of pixels in the basin, Table A3) shows (Figure 9ab) relatively unbiased errors with MAE values close to the means (Table 3), but SWE biases become positive with increasing

310   canopy cover for SPIReS-MODIS, yet negative for SCAG-Fusion and for SPIReS-HLS (except for the highest canopy fractions which contain only 5% of the basin's pixel, Table A3).
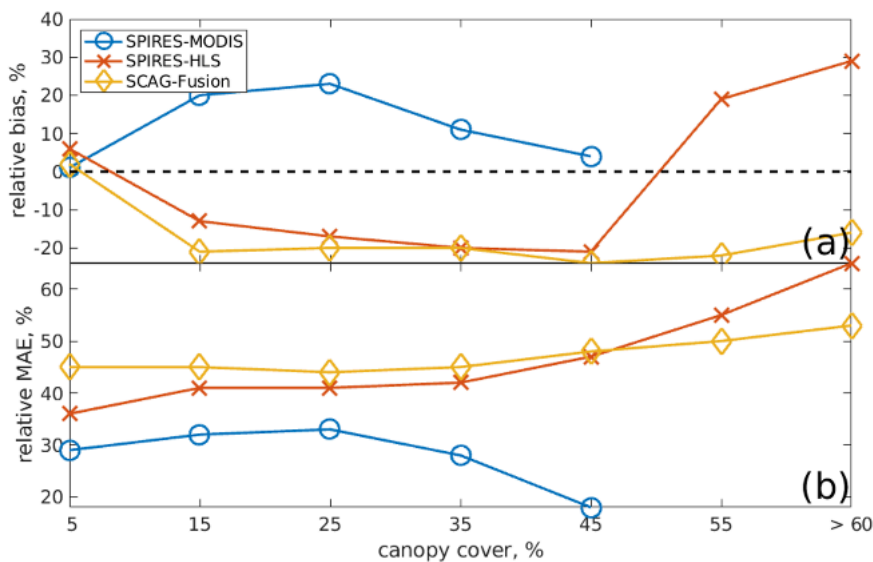
Figure 9:

SWE errors for all dates for the three SWE reconstructions binned by canopy cover percent. Labeled are the bin centers. The relative bias is shown in (a), the relative MAE in (b).

The bias and MAE with increasing canopy cover for SPIReS-HLS and SCAG-Fusion SWE reconstructions are similar to errors in fsca from Landsat 8 (Figure 4c, Stillinger et al., 2022). These fsca biases have similar shapes to the SWE biases indicating these fsca errors cause the SWE errors. Conversely, SPIReS-MODIS shows unbiased fsca with increasing canopy cover (Figure 5d, Stillinger et al., 2022), indicating some other source of error in the SPIReS-MODIS SWE reconstructions.

In summary, the answer to the question posed by the title of this study is yes, as the bias–arguably the most important error statistic for water resource management–was 4-5% lower using the finer resolution snow cover forcings. However, the results are mixed relative to previous studies. For example, Durand et al. (2008) and Molotch and Margulis (2008) report both lower MAE and bias with a 30 m Landsat ETM+ snow cover forcing compared to snow cover from MODIS and AVHRR. The explanation for why some previous studies showed more significant improvements going from moderate to high resolution forcings may be the snow mapping algorithms used. An accurate technique for dealing with mixed pixels is particularly important for moderate resolution sensors since in for mid-latitude mountains most pixels are mixed at 500 m (Selkowitz et al., 2014). In Durand et al. (2008) and Molotch and Margulis (2008), the finer resolution Landsat ETM+ snow cover used a spectral unmixing technique (Painter et al., 2003), but the MODIS snow cover was based on the Normalized Snow Difference Technique, which only uses two bands, versus all available for spectral unmixing, and is shown to have higher MAE and bias (Stillinger et al., 2023). In Cline et al. (1998), the only other study to specifically examine spatial scale with SWE reconstruction, a spectral mixture technique was used on 30 m Landsat ETM+ to produce snow cover estimates (Rosenthal and Dozier, 1996). In that study, the coarsened results produced basin-wide SWE above and below the control simulation used as validation, suggesting that coarsening components of the energy balance did not show a clear trend in error. The snow cover used in that study is shown to have low bias and other measures of error from [0-1] fsca (Rosenthal and Dozier, 1996), thus reducing errors from mixed pixels. Increased spatial and temporal resolution through sensor design, fusion techniques, and satellite constellations are the future of Earth observations, but this study shows how a moderate resolution sensor such as MODIS still offers value for snow mapping and modeling.

4. Conclusion

Optimal resolution questions are fundamental to the global study of snow and will inform future scientific priorities and mission specifications. Increasing spatial and temporal resolution mark remote sensing achievements with the implicit assumption that finer resolution provides greater accuracy. To test this assumption for snow hydrology, an energy balance SWE reconstruction model was run at two different spatial resolutions using three different snow cover forcings. Contrary to previous work, the baseline case using SPIReS-MODIS, a daily 463 m product, showed a lower MAE–a measure of per-pixel accuracy–compared to SCAG-Fusion and SPIReS-HLS, both with 30 m spatial resolution. The SPIReS-HLS showed the

345 lowest bias, however the differences in the errors between all three products may be within the uncertainty caused by scaling artifacts such as basin boundary delineation. The improved bias with increasing spatial resolution, arguably the most important measure for water management, is a promising result; however the increased MAE with finer spatial resolution suggests that the daily acquisitions from MODIS with finer *temporal* resolution provide additional accuracy and/or that there are downscaling limitations with relatively coarse reanalysis data e.g., 10^5 m ($1°$) downscaled to 30 m. Improvements such as the

350 inclusion of Landsat 9 and version 2.0 of the HLS data may improve some of the errors. Future satellite missions that leverage existing and planned constellations such as Landsat Next will improve revisit times, as gaps between observations are still an issue for the HLS data. In summary, conclusions are: 1) Spectrally unmixed snow cover and snow albedo from MODIS continues to provide accurate forcings for snow models and 2) increased spatial and temporal resolution through sensor design, fusion techniques, and satellite constellations are the future of Earth observations, but existing moderate resolution sensors

355 still offer value.

Code availability

The codes for ParBal and SPIReS are available on GitHub: https://github.com/edwardbair

The code for SCAG products is not available

360 **Data availability**

If accepted, the three snow cover products plus their reconstructions will be placed in a publicly accessible repository such as Dryad (https://datadryad.org). For the review process, the HDF5 datasets of snow cover and reconstructions are hosted on an FTP site.

365 SPIReS-MODIS: The snow cover is part of a daily Western US product covering 2001-2021 (Bair and Stillinger, 2022). The reconstructions are available at ftp://ftp.snow.ucsb.edu/pub/org/snow/products/ParBal/WUS/SPIRESforced

SPIReS-HLS: The snow cover and reconstructions are at: ftp://ftp.snow.ucsb.edu/pub/org/snow/products/ParBal /Tuolumne/spires-hls

370

SCAG-Fusion: The snow cover and reconstructions are at:

ftp://ftp.snow.ucsb.edu/pub/org/snow/products/ParBal/Tuolumne/scag-fusion

Author contribution

375 According to CRediT taxonomy:

EHB - all 14 contributor roles

JD - Conceptualization, writing (review & editing)

KR - Conceptualization, data curation, formal analysis, funding acquisition, methodology, resources, writing (review & editing)

380 TS - Investigation, writing (review & editing)

WK - Data curation, formal analysis, investigation, methodology, software, supervision

RED - Resources, funding acquisition

Competing interests

The first author is a member of The Cryosphere Editorial Board.

385 **Acknowledgements**

390

References

Baba, M. W., Gascoin, S., Kinnard, C., Marchane, A., and Hanich, L.: Effect of digital elevation model resolution on the simulation of the snow cover evolution in the High Atlas, Water Resources Research, 55, 5360-5378, 10.1029/2018WR023789, 2019.

395

Bair, E. H., Dozier, J., Davis, R. E., Colee, M. T., and Claffey, K. J.: CUES – A study site for measuring snowpack energy balance in the Sierra Nevada, Frontiers in Earth Science, 3, 58, 10.3389/feart.2015.00058, 2015.

Bair, E. H., Rittger, K., Davis, R. E., Painter, T. H., and Dozier, J.: Validating reconstruction of snow water equivalent in California's Sierra Nevada using measurements from the NASA Airborne Snow Observatory, Water Resources Research, 52, 8437-8460, 10.1002/2016WR018704, 2016.

400

Bair, E. H., Abreu Calfa, A., Rittger, K., and Dozier, J.: Using machine learning for real-time estimates of snow water equivalent in the watersheds of Afghanistan, The Cryosphere, 12, 1579-1594, 10.5194/tc-12-1579-2018, 2018.

405

Bair, E. H., Rittger, K., Skiles, S. M., and Dozier, J.: An examination of snow albedo estimates from MODIS and their impact on snow water equivalent reconstruction, Water Resources Research, 55, 7826-7842, 10.1029/2019wr024810, 2019.

410 Bair, E. H., Stillinger, T., and Dozier, J.: Snow Property Inversion from Remote Sensing (SPIReS): A generalized multispectral unmixing approach with examples from MODIS and Landsat 8 OLI, IEEE Transactions on Geoscience and Remote Sensing, 59, 10.1109/TGRS.2020.3040328, 2021.

Bair, E. H., Dozier, J., Stern, C., LeWinter, A., Rittger, K., Savagian, A., Stillinger, T., and Davis, R. E.: Divergence of
415 apparent and intrinsic snow albedo over a season at a sub-alpine site with implications for remote sensing, The Cryosphere, 16, 1765-1778, 10.5194/tc-16-1765-2022, 2022.

Baumgartner, M. F., Seidel, K., and Martinec, J.: Toward snowmelt runoff forecast based on multisensor remote-sensing informnation, IEEE Transactions on Geoscience and Remote Sensing, GE-25, 746-750, 10.1109/TGRS.1987.289744,
420 1987.

Blöschl, G.: Scaling issues in snow hydrology, Hydrological Processes, 13, 2149-2175, 10.1002/(SICI)1099-1085(199910)13:14/15<2149::AID-HYP847>3.0.CO;2-8, 1999.

425 Bouamri, H., Kinnard, C., Boudhar, A., Gascoin, S., Hanich, L., and Chehbouni, A.: MODIS does not capture the spatial heterogeneity of snow cover induced by solar radiation, Frontiers in Earth Science, 9, 10.3389/feart.2021.640250, 2021.

Claverie, M., Ju, J., Masek, J. G., Dungan, J. L., Vermote, E. F., Roger, J. C., Skakun, S. V., and Justice, C.: The harmonized Landsat and Sentinel-2 surface reflectance data set, Remote Sens Environ, 219, 145-161, 10.1016/j.rse.2018.09.002,
430 2018.

Cline, D., Elder, K., and Bales, R.: Scale effects in a distributed snow water equivalence and snowmelt model for mountain basins, Hydrological Processes, 12, 1527-1536, 10.1002/(SICI)1099-1085(199808/09)12:10/11<1527::AID-HYP678>3.0.CO;2-E, 1998.

435

Conner, M. M., Stephenson, T. R., German, D. W., Monteith, K. L., Few, A. P., and Bair, E. H.: Survival analysis: Informing recovery of Sierra Nevada bighorn sheep, The Journal of Wildlife Management, 82, 1442-1458, 10.1002/jwmg.21490, 2018.

440   Cort, J. W., and Kenji, M.: Advantages of the mean absolute error (MAE) over the root mean square error (RMSE) in assessing average model performance, Climate Research, 30, 79-82, 2005.

Dozier, J., Painter, T. H., Rittger, K., and Frew, J. E.: Time-space continuity of daily maps of fractional snow cover and albedo from MODIS, Advances in Water Resources, 31, 1515-1526, 10.1016/j.advwatres.2008.08.011, 2008.

445

Durand, M., Molotch, N. P., and Margulis, S. A.: Merging complementary remote sensing datasets in the context of snow water equivalent reconstruction, Remote Sens Environ, 112, 1212-1225, 10.1016/j.rse.2007.08.010, 2008.

Foga, S., Scaramuzza, P. L., Guo, S., Zhu, Z., Dilley, R. D., Beckmann, T., Schmidt, G. L., Dwyer, J. L., Joseph Hughes, M.,
450   and Laue, B.: Cloud detection algorithm comparison and validation for operational Landsat data products, Remote Sens Environ, 194, 379-390, 10.1016/j.rse.2017.03.026, 2017.

Hall, D. K., Riggs, G. A., Salomonson, V. V., DiGirolamo, N. E., and Bayr, K. J.: MODIS snow-cover products, Remote Sens Environ, 83, 181-194, 10.1016/S0034-4257(02)00095-0, 2002.

455

Lapo, K. E., Hinkelman, L. M., Sumargo, E., Hughes, M., and Lundquist, J. D.: A critical evaluation of modeled solar irradiance over California for hydrologic and land surface modeling, Journal of Geophysical Research: Atmospheres, 122, 299-317, 10.1002/2016JD025527, 2017.

460   Li, J., and Roy, D. P.: A global analysis of Sentinel-2A, Sentinel-2B and Landsat-8 data revisit intervals and implications for terrestrial monitoring, Remote Sensing, 9, 902, 10.3390/rs9090902, 2017.

Liston, G. E., Haehnel, R. B., Sturm, M., Hiemstra, C. A., Berezovskaya, S., and Tabler, R. D.: Instruments and methods: Simulating complex snow distributions in windy environments using SnowTran-3D, Journal of Glaciology, 53, 241-256,
465   10.3189/172756507782202865, 2007.

Luce, C. H., Tarboton, D. G., and Cooley, K. R.: The influence of the spatial distribution of snow on basin-averaged snowmelt, Hydrological Processes, 12, 1671-1683, 10.1002/(SICI)1099-1085(199808/09)12:10/11<1671::AID-HYP688>3.0.CO;2-N, 1998.

470

MathWorks: MATLAB Mapping Toolbox 5.4: User's Guide, The MathWorks, Natick, MA, 814 pp., 2022.

Molotch, N. P., and Margulis, S. A.: Estimating the distribution of snow water equivalent using remotely sensed snow cover data and a spatially distributed snowmelt model: A multi-resolution, multi-sensor comparison, Advances in Water
475   Resources, 31, 1503-1514, 10.1016/j.advwatres.2008.07.017, 2008.

Painter, T. H., Dozier, J., Roberts, D. A., Davis, R. E., and Green, R. O.: Retrieval of subpixel snow-covered area and grain size from imaging spectrometer data, Remote Sens Environ, 85, 64-77, 10.1016/S0034-4257(02)00187-6, 2003.

20

480   Painter, T. H., Rittger, K., McKenzie, C., Slaughter, P., Davis, R. E., and Dozier, J.: Retrieval of subpixel snow-covered area, grain size, and albedo from MODIS, Remote Sens Environ, 113, 868-879, 10.1016/j.rse.2009.01.001, 2009.

Painter, T. H., Bryant, A. C., and Skiles, S. M.: Radiative forcing by light absorbing impurities in snow from MODIS surface reflectance data, Geophysical Research Letters, 39, L17502, 10.1029/2012GL052457, 2012.

485

Painter, T. H., Berisford, D. F., Boardman, J. W., Bormann, K. J., Deems, J. S., Gehrke, F., Hedrick, A., Joyce, M., Laidlaw, R., Marks, D., Mattmann, C., McGurk, B., Ramirez, P., Richardson, M., Skiles, S. M., Seidel, F. C., and Winstral, A.: The Airborne Snow Observatory: Fusion of scanning lidar, imaging spectrometer, and physically-based modeling for mapping snow water equivalent and snow albedo, Remote Sens Environ, 184, 139-152, 10.1016/j.rse.2016.06.018,

490   2016.

Pflug, J. M., Hughes, M., and Lundquist, J. D.: Downscaling snow deposition using historic snow depth patterns: diagnosing limitations from snowfall biases, winter snow losses, and interannual snow pattern repeatability, Water Resources Research, 57, e2021WR029999, 10.1029/2021WR029999, 2021.

495

Raleigh, M. S., Lundquist, J. D., and Clark, M. P.: Exploring the impact of forcing error characteristics on physically based snow simulations within a global sensitivity analysis framework, Hydrol. Earth Syst. Sci., 19, 3153-3179, 10.5194/hess-19-3153-2015, 2015.

500   Rittger, K., Painter, T. H., and Dozier, J.: Assessment of methods for mapping snow cover from MODIS, Advances in Water Resources, 51, 367-380, 10.1016/j.advwatres.2012.03.002, 2013.

Rittger, K., Bair, E. H., Kahl, A., and Dozier, J.: Spatial estimates of snow water equivalent from reconstruction, Advances in Water Resources, 94, 345-363, 10.1016/j.advwatres.2016.05.015, 2016.

505

Rittger, K., Raleigh, M. S., Dozier, J., Hill, A. F., Lutz, J. A., and Painter, T. H.: Canopy adjustment and improved cloud detection for remotely sensed snow cover mapping, Water Resources Research, 56, e2019WR024914, 10.1029/2019WR024914, 2020.

510   Rittger, K., Krock, M., Kleiber, W., Bair, E. H., Brodzik, M. J., Stephenson, T. R., Rajagopalan, B., Bormann, K. J., and Painter, T. H.: Multi-sensor fusion using random forests for daily fractional snow cover at 30 m, Remote Sens Environ, 264, 112608, 10.1016/j.rse.2021.112608, 2021.

Rodell, M., Houser, P. R., Jambor, U., Gottschalck, J., Mitchell, K., Meng, C. J., Arsenault, K., Cosgrove, B., Radakovich, J., Bosilovich, M., Entin, J. K., Walker, J. P., Lohmann, D., and Toll, D.: The Global Land Data Assimilation System,

515   Bulletin of the American Meteorological Society, 85, 381-394, 10.1175/BAMS-85-3-381, 2004.

Rosenthal, W., and Dozier, J.: Automated mapping of montane snow cover at subpixel resolution from the Landsat Thematic Mapper, Water Resources Research, 32, 115-130, 10.1029/95WR02718, 1996.

520

Rutan, D. A., Kato, S., Doelling, D. R., Rose, F. G., Nguyen, L. T., Caldwell, T. E., and Loeb, N. G.: CERES synoptic product: Methodology and validation of surface radiant flux, Journal of Atmospheric and Oceanic Technology, 32, 1121-1143, 10.1175/JTECH-D-14-00165.1, 2015.

525 Schlögl, S., Marty, C., Bavay, M., and Lehning, M.: Sensitivity of Alpine3D modeled snow cover to modifications in DEM resolution, station coverage and meteorological input quantities, Environmental Modelling & Software, 83, 387-396, 10.1016/j.envsoft.2016.02.017, 2016.

Selkowitz, D. J., Forster, R. R., and Caldwell, M. K.: Prevalence of pure versus mixed snow cover pixels across spatial
530 resolutions in alpine environments, Remote Sensing, 6, 12478-12508, 10.3390/rs61212478, 2014.

Slater, A. G., Barrett, A. P., Clark, M. P., Lundquist, J. D., and Raleigh, M. S.: Uncertainty in seasonal snow reconstruction: Relative impacts of model forcing and image availability, Advances in Water Resources, 55, 165-177, 10.1016/j.advwatres.2012.07.006, 2013.
535
Stillinger, T., Rittger, K., Raleigh, M. S., Michell, A., Davis, R. E., and Bair, E. H.: Landsat, MODIS, and VIIRS snow cover mapping algorithm performance as validated by airborne lidar datasets, The Cryosphere Discuss., 2022, 1-37, 10.5194/tc-2022-159, 2022.

540 Stillinger, T., Rittger, K., Raleigh, M. S., Michell, A., Davis, R. E., and Bair, E. H.: Landsat, MODIS, and VIIRS snow cover mapping algorithm performance as validated by airborne lidar datasets, The Cryosphere, 17, 567-590, 10.5194/tc-17-567-2023, 2023.

Stillinger, T. C.: Observing Snow from Space: Snow/Cloud Discrimination and Opportunities in Water Supply Forecasting,
545 University of California, Santa Barbara, United States -- California, 152 pp., 2019.

Storey, J., Roy, D. P., Masek, J., Gascon, F., Dwyer, J., and Choate, M.: A note on the temporary misregistration of Landsat-8 Operational Land Imager (OLI) and Sentinel-2 Multi Spectral Instrument (MSI) imagery, Remote Sens Environ, 186, 121-122, 10.1016/j.rse.2016.08.025, 2016.
550
Tan, B., Woodcock, C. E., Hu, J., Zhang, P., Ozdogan, M., Huang, D., Yang, W., Knyazikhin, Y., and Myneni, R. B.: The impact of gridding artifacts on the local spatial properties of MODIS data: Implications for validation, compositing, and band-to-band registration across resolutions, Remote Sens Environ, 105, 98-114, 10.1016/j.rse.2006.06.008, 2006.

555 Turpin, O. C., Caves, R. G., Ferguson, R. I., and Johansson, B.: Verification of simulated snow cover in an Arctic basin using satellite-derived snow-cover maps, Annals of Glaciology, 31, 391-396, 10.3189/172756400781819932, 2000.

Vermote, E., Justice, C., Claverie, M., and Franch, B.: Preliminary analysis of the performance of the Landsat 8/OLI land surface reflectance product, Remote Sens Environ, 185, 46-56, 10.1016/j.rse.2016.04.008, 2016.
560
Vuyovich, C. M., Deeb, E. J., Polashenski, C., Courville, Z., Hiemstra, C. A., Wagner, A. M., Eylander, J. B., and Davis, R. E.: Snow Strategic Science Plan, ERDC/CRREL, Hanover, NH, 91, 2018.

Winstral, A., Marks, D., and Gurney, R.: Assessing the sensitivities of a distributed snow model to forcing data resolution,
565 Journal of Hydrometeorology, 15, 1366-1383, 10.1175/jhm-d-13-0169.1, 2014.

22

Wolfe, R. E., Roy, D. P., and Vermote, E.: MODIS land data storage, gridding, and compositing methodology: Level 2 grid, IEEE Transactions on Geoscience and Remote Sensing, 36, 1324-1338, 10.1109/36.701082, 1998.

570 Xia, Y., Mitchell, K., Ek, M., Sheffield, J., Cosgrove, B., Wood, E., Luo, L., Alonge, C., Wei, H., Meng, J., Livneh, B., Lettenmaier, D., Koren, V., Duan, Q., Mo, K., Fan, Y., and Mocko, D.: Continental-scale water and energy flux analysis and validation for the North American Land Data Assimilation System project phase 2 (NLDAS-2): 1. Intercomparison and application of model products, Journal of Geophysical Research: Atmospheres, 117, D03109, 10.1029/2011JD016048, 2012.

575

Appendix A

Name	Year	Bias, mm	Relative Bias, %	MAE, mm	Relative MAE, %
SPIReS-MODIS	2018	9	3	87	32
	2019	26	4	168	26
	2020	43	21	95	47
	mean	**26**	**9**	**117**	**35**
SPIReS-HLS	2018	40	15	140	52
	2019	-6	-1	194	31
	2020	26	13	100	50
	mean	**20**	**9**	**145**	**44**
SCAG-Fusion	2018	1	0	90	33
	2019	-108	-17	221	35
	2020	52	26	97	48
	mean	**-18**	**3**	**136**	**39**

Table A1:

Error statistics by date for the three SWE reconstructions, but with all pixels upscaled to 2000 m. The SPIRES-MODIS rows
580 *are identical to those in Table 2 and are shown for comparison.*

Name	Date	Bias, mm	Bias, %	MAE, mm	MAE, %
SPIReS-MODIS	23 Apr 2018	38	9	107	25
	28 May 2018	-20	-16	68	53
	17 Apr 2019	79	7	228	21
	03 May 2019	111	13	223	26
	13 Jun 2019	-66	-15	150	33

Name	Date	Bias, mm	Bias, %	MAE, mm	MAE, %
	05 Jul 2019	-22	-19	70	61
	13 Apr 2020	137	47	150	51
	07 May 2020	13	7	76	40
	21 May 2020	-21	-17	59	48
SPIReS-HLS	23 Apr 2018	51	12	225	53
	28 May 2018	3	3	46	36
	17 Apr 2019	-32	-3	336	30
	03 May 2019	28	3	284	33
	13 Jun 2019	-79	-18	142	32
	05 Jul 2019	-10	-9	41	36
	13 Apr 2020	84	28	175	59
	07 May 2020	-14	-7	95	49
	21 May 2020	-33	-26	63	49
SCAG-Fusion	23 Apr 2018	15	4	164	39
	28 May 2018	10	8	80	63
	17 Apr 2019	-169	-15	419	38
	03 May 2019	-70	-8	338	40
	13 Jun 2019	-105	-24	216	49
	05 Jul 2019	-13	-11	81	72
	13 Apr 2020	131	44	185	62
	07 May 2020	23	12	111	58
	21 May 2020	-3	-2	74	57

Table A2:

Error statistics by date for the three SWE reconstructions.

Name	Canopy cover, %	Pixels, number	Pixels, %	Bias, mm	Bias, %	MAE, mm	MAE, %
SPIReS-MODIS	5	131	46	7	1	155	29
	15	76	27	68	20	111	32
	25	38	13	57	23	81	33
	35	25	9	23	11	62	28
	45	8	3	8	4	36	18
	55	0	0				
	> 60	0	0				

	5	48230	60	27	6	167	36
SPIReS-HLS	15	8737	11	-45	-13	143	41
	25	6553	8	-59	-17	137	41
	35	6969	9	-64	-20	132	42
	45	5760	7	-59	-21	133	47
	55	2869	4	52	19	152	55
	> 60	962	1	73	29	165	65
SCAG-Fusion	5	48230	60	11	2	212	45
	15	8737	11	-74	-21	156	45
	25	6553	8	-67	-20	148	44
	35	6969	9	-63	-20	141	45
	45	5760	7	-70	-24	137	48
	55	2869	4	-60	-22	136	50
	> 60	962	1	-41	-16	135	53

Table A3:

585 *Error statistics by canopy cover, for all dates, for the three SWE reconstructions.*